Nano Research

ISSN 1998-0124 CN 11-5974/O4
https://doi.org/10.1007/s12274-024-6671-9

Research Article

Enhanced photoluminescence of a microporous quantum dot color conversion layer by inkjet printing

Junchi Chen[1], Qihao Jin[1], Yidenekachew. J. Donie[2], Orlando. T. Perales[1], Dmitry Busko[3], Bryce. S. Richards[3], and Uli Lemmer[1,3] (✉)

[1] *Light Technology Institute (LTI), Karlsruhe Institute of Technology (KIT), Engesserstrasse 13, 76131 Karlsruhe, Germany*
[2] *Department of Chemical Engineering and Materials Science, University of Minnesota (UMN), 421 Washington Ave. SE, Minneapolis, MN 55455-0132, USA*
[3] *Institute for Microstructure Technology, Karlsruhe Institute of Technology (KIT), Hermann-von-Helmholtz-Platz 1, 76344 Eggenstein-Leopoldshafen, Germany*

Received: 29 June 2023 / **Revised:** 12 March 2024 / **Accepted:** 30 March 2024

ABSTRACT

Owing to their high color purity, tunable bandgap, and high efficiency, quantum dots (QDs) have gained significant attention as color conversion materials for high-end display applications. Moreover, inkjet-printed QD pixels show great potential for realizing full-color mini/micro-light emitting diode (micro-LED)-based displays. As a color conversion layer, the photoluminescence intensity of QDs is limited by the insufficient absorptance of the excitation light due to the lack of scattering. Conventional scatterers, such as titanium dioxide microparticles, have been applied after additional surface engineering for sufficient dispersity to prevent nozzle clogging in inkjet printing process. In our work, as an alternative approach, we use inkjet printing for depositing a phase separating polymer ink based on polystyrene (PS) and polyethylene glycol (PEG). QD/polymer composite pixels with scattering micropores are realized. The morphology of the micropores can be tailored by the weight ratio between PS and PEG which enables the manipulation of scattering capability. With the presence of the microporous structure, the photoluminescence intensity of the QD film is enhanced by 110% in drop-cast films and by 35.3% in inkjet-printed QD pixel arrays compared to the reference samples.

KEYWORDS

porous structure, inkjet printing, phase separation, quantum dots, display technology

1 Introduction

In recent years, quantum dots (QDs) have emerged as promising emissive materials with the potential to replace conventional rare-earth phosphors in display and lighting applications [1, 2]. Owing to their tunable band gap, small full-width-at-half-maximum (FWHM) of the emission spectrum, and high photoluminescence quantum yield (PLQY), QD materials are capable of empowering greater purity of each primary color and boosting the efficiency of display devices [3, 4]. Commercially, the integration of QD color conversion layer with liquid crystal display technology has successfully captured a significant market share in recent years [5]. On the other hand, micro-light emitting diodes (micro-LEDs) have been developing rapidly and are regarded as a game-changing technology for display applications [6, 7]. QD materials show great potential as a color conversion layer in micro-LED-based full-color displays. Compared to micrometer-scale rare-earth phosphors, QD materials have significantly smaller particle sizes, falling within the nanometer range. This allows for a more uniform coating of micro-LED chips. Moreover, the smaller particle size enables better adaptivity to micro-patterning processes like inkjet printing [8, 9] and photolithography [10, 11], increasing the potential for mass production.

QD materials are normally packaged in a polymeric or inorganic matrix to acquire better stability and lifetime in practical applications [12, 13]. As a color conversion layer, the overall photoluminescence (PL) intensity of QD is remarkably dependent on the absorption of the excitation light. However, due to the small particle size, QDs cannot generate sufficient optical scattering resulting in a short optical path length of the excitation light inside the layer and a low probability of being absorbed by the QDs [14]. Besides, the poor light extraction of the color conversion layer is another obstacle to high efficiency [15]. Due to the total internal reflection, part of the emitted light from the QDs is trapped in the matrix and gradually vanishes due to reabsorption.

Addressing the problems above, various scattering media including nano- or micro-particles [16–18], surface scattering texture [19, 20], porous scattering structure [21, 22], and diffusing back-reflector [23, 24], have been incorporated into the QD color conversion layer for improving absorption and light extraction. Among them, the introduction of a disordered porous scattering structure is a low-cost and efficient method to obtain broadband light scattering generated by the pores with irregular sizes and morphologies. To fabricate this type of structure, a rapid method based on supercritical CO_2 foaming was exploited to form a

Address correspondence to uli.lemmer@kit.edu

microporous network in QD/poly(methyl methacrylate) hybrid film achieving a strong enhancement in PL intensity [25]. As an alternative method, a humidity-controlled approach to self-assemble hierarchical porous structure in QD/block copolymer composite film was proposed, exhibiting pronounced enhancements in both light absorption and extraction efficiency [26]. However, both above-mentioned fabrication approaches require complex equipment and bring problematic environments to QD material, such as high temperature or high humidity [27, 28]. Moreover, the existing approaches only practically test with QD films instead of micropatterned QD pixels which are essential in display technology. Thus, fabricating methods for porous structures with a possibility for depositing pixelated QD color converters with a high yield are needed. Owing to the advantages of being material-efficient, mask-free, and contactless, inkjet printing has been widely investigated and applied to QD pixelation [29, 30] and other optical components [31–33].

In this study, inkjet printing of a phase separating ink based on polystyrene (PS) and polyethylene glycol (PEG) blend is proposed for fabricating microporous structure in QD/polymer composite. This approach demonstrates distinct advantages over directly embedding optically scattering particles, as these scattering particles with relatively large size tend to block the inkjet printing nozzle. The microporous structure is generated spontaneously by the sequential solidification of PS-rich and PEG-rich domains during solvent volatilization [34, 35]. The morphology of the microporous network can be conveniently manipulated by the weight ratio of PS and PEG, providing fine control over the optical scattering properties of the network. Based on this method, the microporous QD film prepared by drop-casting reveals a substantial enhancement in PL intensity. Moreover, as a solution-based process, this phase separation approach is highly compatible with inkjet printing technique for the cost-efficient mass production of microporous QD pixels for display applications. With further optimization of the ink, a uniform dot array of microporous QD pixels with a diameter of around 30 μm was fabricated by inkjet printing and showed a remarkable PL intensity enhancement of 35.3%.

2 Results and discussion

The process of preparing microporous QD/polymer composites is illustrated in Fig. 1(a). To obtain the solution of the polymer blends, PS and PEG powder with desired weight ratio are first added into a common solvent (chloroform for drop-casting, 1,2-dichlorobenzene for inkjet printing) followed by 2 h of magnetic stirring. After the complete dissolution of the polymers, QD powder or dispersion is added into the polymer blend solution and mixed homogeneously. To fabricate microporous QD films, the obtained solution is drop-cast on a glass substrate that has been treated in oxygen plasma for 3 min. The solution is then solidified along with solvent volatilization under a glass cover to avoid the impact of ambient gas flow. During the solvent volatilization, as shown in the inserts, the solution gradually forms PS-rich and PEG-rich domains. As the solubility of PS in the solvent is poorer than PEG, the PS-rich domains solidify faster and form the outer framework. At this moment, the PEG-rich domains are still in a liquid phase and embedded in the PS framework. After the solvent volatilizes completely, PEG-rich domains solidify as well and collapse inside the PS matrix generating massive air voids.

To fabricate microporous QD pixels, the obtained solution is

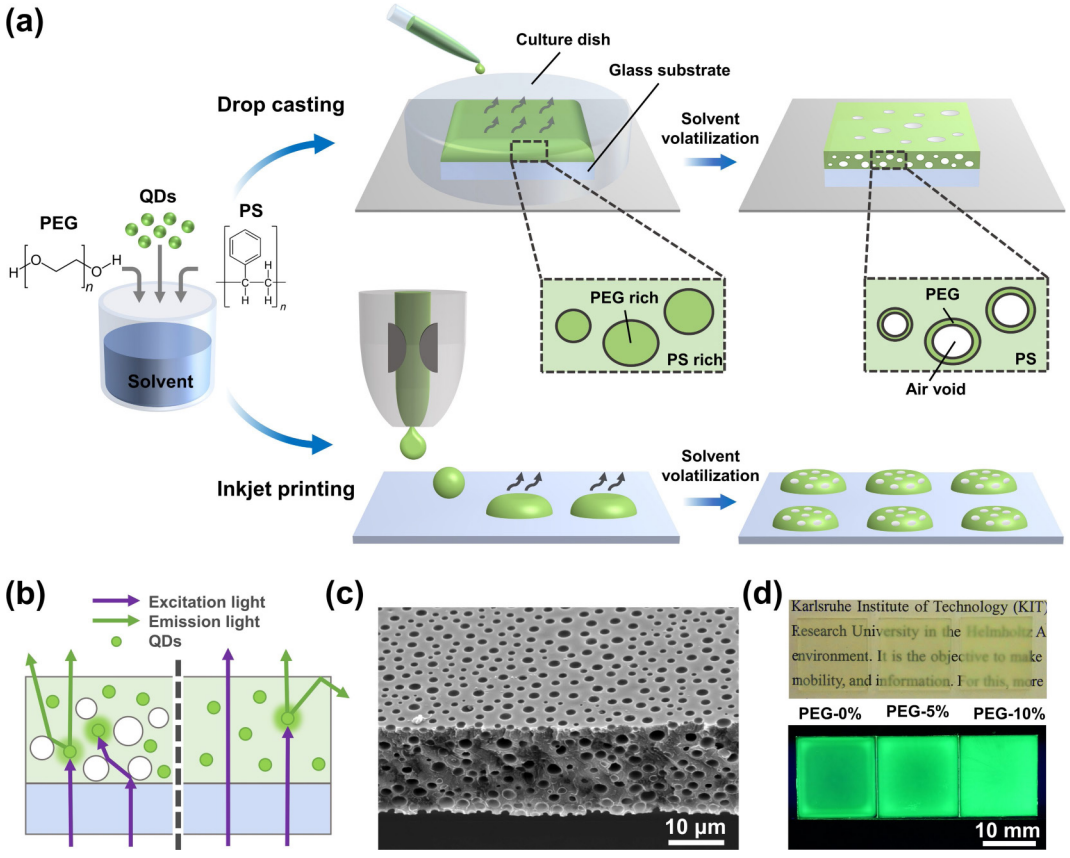

Figure 1 (a) Schematics of the fabrication process for microporous QD films and inkjet-printed micro-pixels, respectively. The inserts are illustrations of the phase separation process of the PS/PEG polymer blends during solvent volatilization. (b) Scheme of optical mechanisms: Scattering leads to an elongated optical path length of excitation light in QD/polymer composite and the enhanced light extraction caused by micropores. (c) SEM image (45° tilted) of a microporous QD film (PEG-20%). (d) Photographs of QD/polymer films with different PEG mass fractions under ambient white light (upper row) and 365 nm UV radiation (bottom row) illuminated from the bottom.

applied as the ink for the inkjet printing process and the formation mechanism of the porosity is the same as during the drop-casting process. However, the jetting gas flow and minimized size of the printed droplet during inkjet printing can accelerate the solvent volatilization and the solidification of the polymers. Thus, a solvent with a relatively lower vapor pressure, such as 1,2-dichlorobenzene, is used for preparing the ink. In the inkjet printing process, since the micropore structure is generated after leaving the printing nozzle, the polymer blend ink will not cause any clogging of the nozzle. In this study, the PEG polymer plays the role of the porogen in the phase separation system and the weight ratio between PS and PEG is applied as the key parameter to control the morphology. Thus, we name and distinguish the samples by their PEG mass fraction in the total polymer blend. For instance, "PEG-10%" represents that the sample has a weight ratio between PEG and PS of 1:9. To evaluate the distribution of QDs in the two polymers, a very thin film PEG-50% sample with QDs was prepared by spin coating (2000 rpm, 30 s). The microscopic images obtained under white light and ultraviolet (UV) illumination of the two-dimensional (2D) porous film are shown in Fig. S1 in the Electronic Supplementary Material (ESM). In the images, the PS domains exhibit stronger fluorescence than the PEG domains. A rinsing process in deionized (DI) water was conducted subsequently to distinguish the PS and PEG domains as PEG can be selectively removed by water in this blend system.

The schematic in Fig. 1(b) shows the traces of the exciting UV or blue radiation impinging on the QD/polymer films with (left side) or without micropore structure (right side), respectively. The micropore structure enhances the PL intensity mainly in two aspects: (1) the optical pathlength of the excitation photons inside the color conversion medium is significantly elongated by the scattering effect, thereby increasing the probability of being absorbed by the semiconductor nanoparticles; (2) parts of the emission light that would otherwise be laterally waveguided and trapped is scattered by the micropores and then outcoupled to the vertical direction. Indeed, the enhancement effect of the micropore structure is highly dependent on its morphology including pore size and pore density. Therefore, a fabrication method for porous scattering structures with good control of the morphology is essential for performance optimization when practically applied in optical devices.

Figure 1(c) is the scanning electron microscopy (SEM) image of a microporous QD/polymer film (PEG-20%) at a tilt angle of 45°. This image exhibits the disordered distribution of the volumetric micropores inside the film and on the surface of the film as well. The structure presents a non-uniform shape and diameter. The micropores are the dominant scattering media that enhance the absorption of QDs and are beneficial to improving light extraction. The non-uniform size of the micropores enables broadband scattering and inhibits wavelength dependence. The embedded QDs are not visible in this magnification. We thus conclude that micro-scale aggregation of nanoparticles does not play a role. In Fig. 1(d), photographs of QD/polymer films with different PEG mass fractions (0%, 5%, and 10%) under daylight and 365 nm UV excitation are shown for visual comparison of the scattering properties and PL intensities among the QD films. Under daylight, the QD film without porosity is transparent and shows clearly the letter pattern underneath. With the increase of the PEG mass fraction, the QD films show an increased haze which gradually fuzzes the letter pattern. With the UV excitation from the bottom direction, the PEG-5% and PEG-10% QD films exhibit higher brightness than the PEG-0% sample demonstrating the significant enhancement of forward-luminescence resulting from the micropore structure.

To quantitively investigate the optical performances of the micropore structures, PS/PEG hybrid films with varying PEG mass fractions from 0 wt.% to 30 wt.% were prepared for structural and optical characterization. In this part, QDs were not included in the film to remove their influence on the optical measurement. The film samples were prepared by drop-casting on glass substrates (16 mm × 16 mm) with the same volume of the solution. All the films were solidified at 22 °C with a glass cover to minimize the influence of external airflow. The molecular weight of PS (Sigma-Aldrich) polymer was 100,000 Da and the molecular weight of PEG (Sigma-Aldrich) was 200 Da. To reduce the duration of solvent volatilization, chloroform with a high volatilization rate was selected as the solvent. Details of the solution preparation and drop-casting process are described in the experimental section. Moreover, as the drop-cast microporous films are prone to be non-uniform when the PEG mass fraction is too high, we set 20% as the maximum weight percent in this investigation to ensure the accuracy of the measurement.

The cross-sectional SEM images of the PS/PEG hybrid films are shown in Fig. 2(a). As a reference, the PEG-0% sample shows a smooth cross-section due to the lack of PEG porogen. With the increase of PEG mass fraction, the porosity of the film gradually increases and is mainly reflected in the growth of the pore diameter. The reason is that, during solvent volatilization, the PEG-rich domains maintain their mobility in the polymer blend solution before the solidification of PS-rich domains and keep coalescing with the neighboring domains to form larger droplets until the PS-rich domain is solidified. Thus, the polymer blends with higher PEG mass fraction facilitate more coalescence as the density of PEG-rich domains is higher, resulting in the increase of the final pore size. To statistically show the tendency, the mean diameter of the micropore structure with different PEG mass fractions is extracted from the SEM images and shown in Table 1. The disordered pore size and random distribution of the micropores enable efficient broadband light scattering for visible wavelengths. Moreover, the significant and systematic geometrical variation of the micropore structure verifies that the PEG mass fraction is a convenient and efficient parameter for morphology control. Indeed, besides the mass fraction of PEG, various parameters including curing temperature, molecular weight of the polymers, and solvent type can be adapted to tailor the morphology of the micropores. As an example, the microporous PS/PEG films with the same PEG mass fraction but cured at different temperatures were prepared. Their cross-sectional SEM images are shown in Fig. S2 in the ESM. The result shows a gradual decrease in the pore size and an increase in the pore amount with rising curing temperature.

In Fig. 2(b), the far-field transmission patterns of a blue laser beam passing through a PEG-0% film (left) and a PEG-20% film (right) are presented. The distance between the sample film and the receiving plane is 15 cm. Obviously, the pattern of the laser beam is remarkably broadened by the microporous structure, visually indicating the enhanced scattering performance of PEG-20% film. Figures 2(c) and 2(d) show the transmittance and haze spectra of the microporous films with different PEG mass fractions in the wavelength range of 400–800 nm. In these measurements, the microporous films were separated from the glass substrate as freestanding samples and characterized by a ultraviolet–visible–near-infrared (UV–VIS–NIR) spectrometer (Lambda 1050+ UV–VIS–NIR, PerkinElmer). Here, the haze value is defined as the portion of the diffused transmittance (> 5°) to the overall transmittance. The corresponding mean values (400–800 nm) of the transmittance and haze are listed in Table 1. The transmittance spectra show a gradual decrease with increasing PEG mass fraction. Specifically, the mean transmittance drops from 90.3% for the non-porous film to 73.6% when the mass

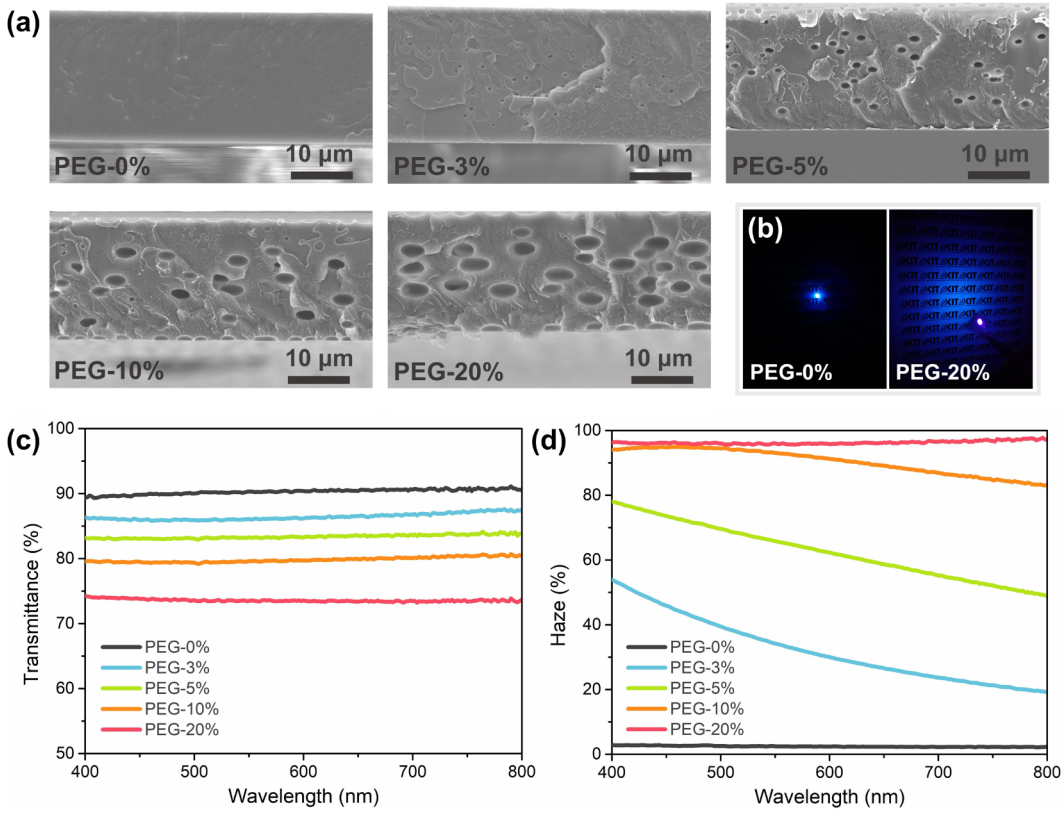

Figure 2 (a) Cross-sectional SEM images of the microporous polymer films with PEG mass fraction ranging from 0% to 20%. (b) Far-field transmission patterns of a blue laser beam passing through PEG-0% and PEG-20% samples, respectively. (c) Transmittance spectra and (d) haze spectra of the microporous polymer films with different PEG mass fractions.

Table 1 Mean diameter of micropores, mean transmittance, and mean haze of the microporous films with different PEG mass fractions

PEG mass fraction (wt.%)	0	3	5	10	20
Mean diameter (μm)	—	0.75	1.76	3.0	4.42
Mean transmittance (%)	90.3	86.4	83.4	79.8	73.6
Mean haze (%)	2.4	32.1	62.6	90.4	96.3

fraction of PEG is 20 wt.%. The reason is that the dense micropore structure causes multiple scattering of the impinging light and part of the incident light is redirected to the backward direction, resulting in a reduction of the transmittance. On the other hand, with the rise of the PEG mass fraction, the average haze values of the films gradually increase from 2.4% to 96.3%. The elevated haze value is due to the enhancement in the scattering performance. In addition, the broad variation range on haze value shows the great adjustability of this fabricating method on the scattering capability. As excessive scattering can cause a reduction in total transmittance, the density of the micropore structure needs to be balanced between the transmission loss and the scattering enhancement in a practical application. Thus, the morphology controllability of the fabrication method is essential. Besides, PEG-3%, PEG-5%, and PEG-10% samples exhibit a degree of wavelength dependence in haze spectra as they contain some pores with a diameter in the sub-micrometer range which are more effective for short wavelengths than for long wavelengths. This phenomenon is consistent with the SEM characterization of their morphology. To describe the scattering performance of the films in more detail, a characterization of the angular intensity distribution (off-axis angle: 0°–75°) of transmitted light was conducted on the sample films mentioned above. A red laser beam (peak wavelength at 640 nm) was chosen as the testing light. The schematic of the home-built measuring system is shown in Fig. S3 in the ESM and the angular distribution curves (normalized to the maximum value) are shown in Fig. S4 in the ESM. In this figure, a broader spreading angle of the transmitted light represents a better scattering capability and was obtained for the films with a larger PEG mass fraction.

To evaluate the influence of the micropore structure on the PL intensity of the QD film in the color conversion process, a group of QD/polymer films with different PEG mass fractions ranging from 0 wt.% to 20 wt.% were prepared and characterized in an integrating sphere system with blue laser excitation (peak wavelength 405 nm). A green-emitting CdSe/ZnS core–shell QD (Beida Jubang Co., Ltd) dispersion was added to the solutions subsequently. The obtained solutions were drop-cast on glass substrates (16 mm × 16 mm) with the same dropping volume. The concentration of QDs was 1 mg/mL and the total polymer concentration was 50 mg/mL in the solution. The thickness of the obtained films was about 25 μm after complete solvent volatilization. Besides, the optical properties of the QD/chloroform dispersions including PLQY, absorbance spectrum, and emission spectra are shown in Fig. S5 in the ESM. The PLQY measurement was based on the 3M method [36, 37]. The scheme of the measuring system is shown as the insert in Fig. 3(a) and more details can be found in Fig. S6 in the ESM. In this measurement, the power of the blue laser was 1.70 mW.

As shown in Fig. 3(a), the peak value of the emission spectrum (in the green range) gradually elevates with the increase of PEG mass fraction. Compared to the PEG-0% sample, the PEG-3% sample shows little enhancement as the density of the micropore is too low to contribute sufficient scattering. The PL enhancement is

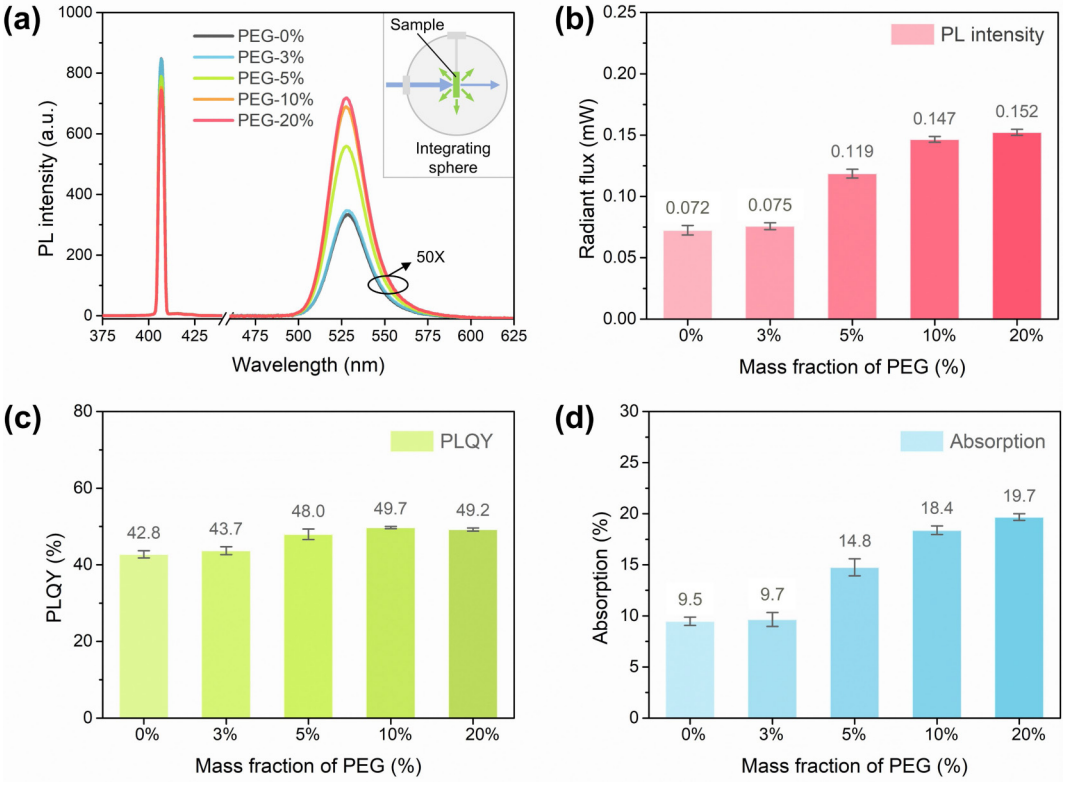

Figure 3 (a) PL spectra, (b) radiant flux of the emission peaks (475–600 nm), (c) PLQY, and (d) absorption of the microporous QD/polymer films with different PEG mass fractions. The insert is the scheme for the PL measurement with an integrating sphere.

more pronounced when the PEG mass fraction is in the range of 5 wt.% to 20 wt.% due to the stronger scattering effect. On the contrary, the peak value of the transmitted excitation light (in the blue spectral range) gradually decreases with the increase of PEG mass fraction. This can be attributed to the increased absorptance of the film. The peak wavelength of the emission remains unchanged among all samples indicating that the phase separation process does not impact the emission properties of the QDs. By integrating the PL intensity over the wavelength range of 475–600 nm, the radiant fluxes of the emission peak of the QD films are calculated and revealed in Fig. 3(b). The PEG-20% sample achieves the maximum radiant flux of 0.152 mW, which is 110.0% higher than the PEG-0% sample (0.072 mW) without microporous structure.

To elucidate the detailed enhancement mechanism, the PLQY, and absorptance of the films were quantitively characterized. Here, the absorption is defined as the percentage of the intensity of the excitation light absorbed by QD film to the total intensity of the excitation light. As shown in Fig. 3(c), the PLQY value first increases with the rising PEG mass fraction and then slightly decreases when the mass fraction is higher than 10 wt.%. Since the emission light from QDs undergoes waveguiding in the encapsulating matrix, the PLQY value is suppressed by reabsorption inside the film [38]. Therefore, the micropores with appropriate density can scatter emitted photons from waveguide modes inside the film and weaken the reabsorption of QD emission. However, excessive light scattering inside the QD film also leads to increased light trapping and thus to reabsorption. The overall effect on PLQY is the result of the competition between these two mechanisms and the best balance is found in the PEG-10% sample exhibiting the highest PLQY. In Fig. 3(d), the film samples with higher PEG mass fraction exhibit significantly larger absorptance. Compared to the PLQY value, the absorption of the sample films shows a stronger correlation to the radiant flux emitted from the samples, which indicates that the enlarged absorption is the dominant factor for luminescence enhancement. Moreover, the transmittance spectrum of a pure PEG layer is shown in Fig. S7 in the ESM, suggesting a low light absorption of the PEG polymer. It indicates that the improvement of the blue light absorption of the QD film is caused by the increased porosity, instead of the elevated PEG concentration. The low light absorption of the encapsulation matrix is beneficial for the color conversion of QD films. Indeed, as the scattering capability of the micropores is generated by the refractive index contrast between air and polymer, it enables a strong scattering effect in a low-refractive-index and low light-absorbing system. The conventional strategies of embedding high-refractive-index particles (e.g. TiO_2-, ZrO_2-, and ZnO-nanoparticles) in polymer film for boosting light scattering commonly results in more severe losses of the excitation light due to higher extinction of the high-refractive-index particles in the blue and UV spectral band [39, 40]. The excitation light absorbed by the scatterers instead of the QDs does not contribute to the PL intensity and reduces the overall efficiency. For comparison, PS films and QD/PS films embedded with various concentrations of TiO_2 nanoparticles (with a diameter of ~ 200 nm) were prepared for optical characterizations via drop-casting. The transmittance and haze spectra of the PS films containing embedded TiO_2 particles are shown in Fig. S8 in the ESM, and the luminescence performances of the TiO_2/QD/PS films are exhibited in Fig. S9 in the ESM. The diameter of the nanoparticles was selected for optimal scattering efficiency for blue light [17, 41]. Compared to the equivalent sample without TiO_2 particles, a maximum radiant flux enhancement of 76.6% is obtained by the QD/PS films containing 10 wt.% TiO_2. The enhancement factor is lower than that of the microporous QD films with PEG as the porogen. For testing the PL enhancing effect of the porous structure for lighting applications, red-, green-, and blue-emitting QD films with different PEG mass fractions (0 wt.%, 5 wt.%, and 10 wt.%) were prepared and placed on a UV chip to realize white LEDs (WLEDs). The electroluminescence (EL) spectra and the scheme of the architecture of the WLEDs are shown in Fig. S10 in the ESM. As a result, compared to the reference sample without

porosity, a maximum luminous efficacy enhancement of 38.4% was obtained for the WLED with microporous structure.

Inkjet printing is a very versatile method for the deposition of patterned functional layers [42]. Furthermore, its use is becoming more widespread for display manufacturing. To demonstrate the compatibility of the proposed phase separation method to inkjet printing, we fabricated QD pixel arrays with microporous structure by inkjet printing and characterized the resulting morphology and optical performance. The preparation of the QD/PS/PEG ink is similar to the procedure for the drop-cast film described above. However, as the jetting behavior of inkjet printing can accelerate the solvent volatilization of the ink and potentially cause nozzle clogging, 1,2-dichlorobenzene with a relatively low vapor pressure was chosen as the ink solvent instead of chloroform. Moreover, PS with a lower molecular weight of 18,000 Da was applied here to reduce the viscosity of the ink while the molecular weight of PEG remained the same (200 Da). The total polymer concentration (PS and PEG) of the ink was 10 mg/mL and the QD concentration was 0.5 mg/mL in the solution. Before printing, a thin polydimethylsiloxane (SYLGARD 184, Sigma-Aldrich) interlayer was spin-coated on the glass substrates (20 mm × 20 mm) to increase the contact angle between the printed ink droplet to improve the printing image. As shown in Fig. S11 in the ESM, a contact angle measurement was conducted for polydimethylsiloxane interlayer and a contact angle of 42.1° was obtained with 1,2-dichlorobenzene solvent. During the inkjet printing, the nozzle temperature was 27 °C and the substrate temperature was 25 °C. The printing resolution was 200 dots per inch. Multiple printing passes (5 passes) were executed for a sample to increase the thickness of the QD pixel.

The atomic force microscopy (AFM) and SEM images of the inkjet-printed QD pixels with different PEG mass fractions are depicted in Figs. 4(a) and 4(b), respectively. The PEG-0% pixel shows a smooth upper surface and a slight sag at the center of the pixel. With the existence of PEG, dense micropores can be observed on the surface of the PEG-10% pixel. Compared to the drop-cast PEG-10% film, the overall pore size of the PEG-10% pixel is smaller and the density of the pores is higher due to the accelerated solvent volatilization. Moreover, since the solvent volatilizes faster at the edge region than at the center region, the solidification of PS starts from the edge to the center of a pixel. This leads to a variation of the pore size and morphology with the smaller pores locating at the edge and the larger pores occurring at the center. This effect is even more pronounced for the PEG-20% pixel. A large void is formed at the center of the pixel due to the excessive coalescence of PEG domains. This also leads to a lower regularity of the pore pattern. From the SEM image, secondary porous structures can be observed on the inner surface of the

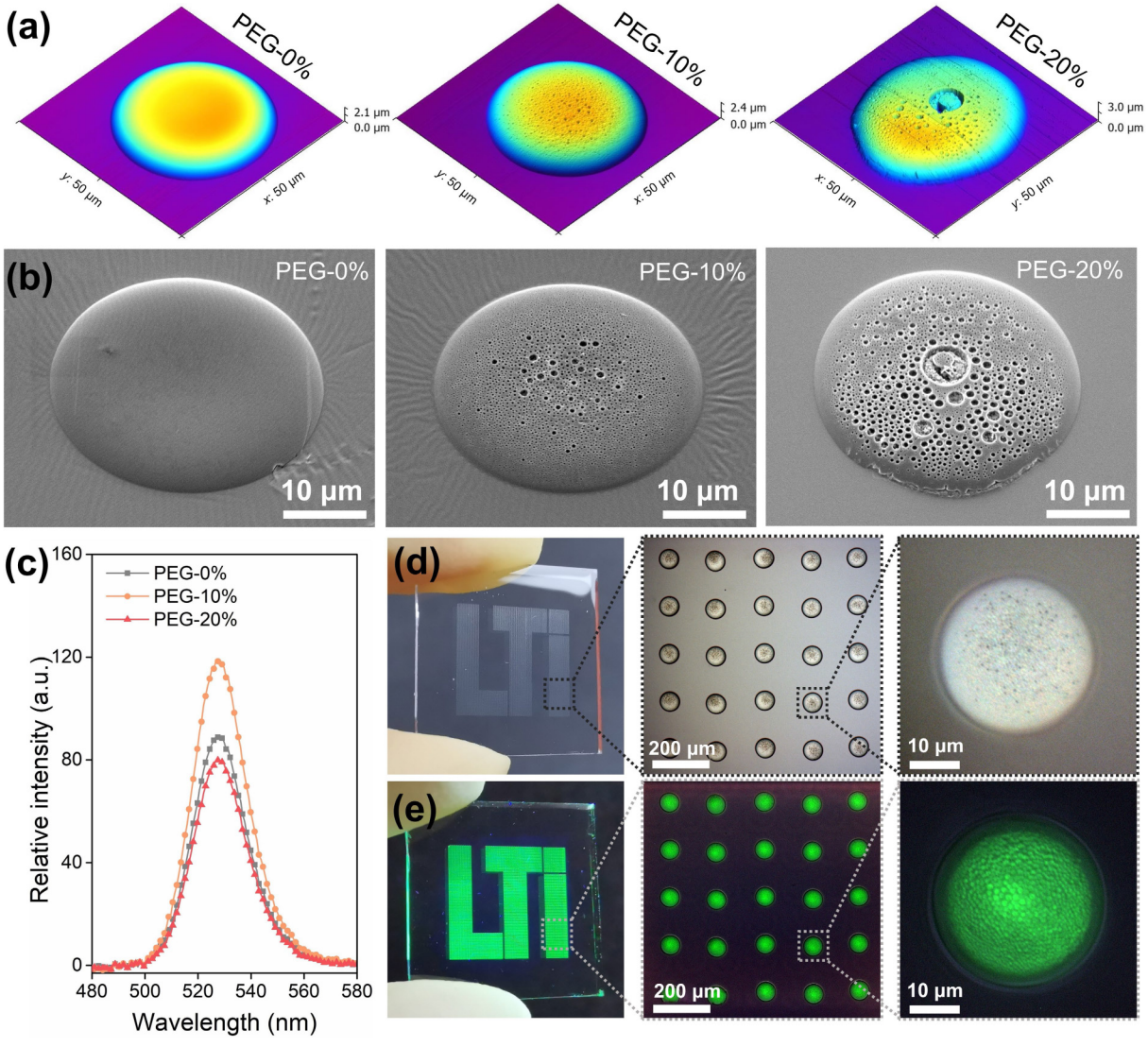

Figure 4 (a) AFM images and (b) SEM images (45° tilted) of inkjet-printed QD pixels with different PEG mass fractions (0%, 10%, and 20%). (c) PL spectra of the QD pixel arrays with different PEG mass fractions. Photographs and optical microscopic images of the inkjet-printed microporous QD pixel array (PEG-10%) under (d) ambient light and (e) 365 nm UV excitation.

micropores, indicating that there is a hierarchy of pores inside the pixel. To investigate the morphological uniformity of the inkjet-printing microporous pixels, 27 QD pixels with different PEG mass fractions are statistically characterized by SEM images. The corresponding frequency distribution diagrams of the diameter of the micropores are shown in Figs. S12–S14 in the ESM.

The optical characterization of the QD pixels is shown in Fig. 4(c). The PL spectra of the printed samples with different PEG mass fractions with the excitation of a blue laser (405 nm) with the same power for all samples are displayed. Compared to the PEG-0% sample, the PEG-10% sample shows a higher emission intensity. The enhancement of the PL intensity is 35.3%. In contrast, the PEG-20% sample shows a lower PL intensity, which is inconsistent with the observation of drop-cast films. Compared to the drop-casting process, the solvent volatilization of the polymer blends is accelerated in inkjet printing, resulting in a denser micropore structure and stronger scattering even with the same PEG mass fraction. Thus, the reduced PL intensity should be attributed to the excessive light scattering which potentially traps the emitted light inside the pixel and generates serious reabsorption. The solvent volatilization also affects the morphology of the pixels. For instance, parts of the micropores at the edge region of the pixel are smaller than the wavelength scale thus generating insufficient scattering. On the other hand, the micropores at the center region might lead to excessive scattering.

As an example of the usability of inkjet printing, we present a microscopic "LTI" pattern based on printed microporous QD pixels (PEG-10%) in Fig. 4(d). Pixels with a dot size of around 30 μm are fabricated with a regular round shape and uniformity. With higher magnification, the dense and disordered micropores can be observed on the pixel. Fig. 4(e) shows the fluorescence images of the QD pixels excited with UV radiation (365 nm) from the bottom. From these microscopic images, a higher fluorescence intensity appears at the locations with micropores. Many bright circular spots can be observed. This can be attributed to the improved light extraction caused by the micropores on the pixel surface. Besides, good fluorescence uniformity is achieved among the printed pixels. The gray scale profiles of the fluorescent image in Fig. 4(e) are extracted and shown in Fig. S15 in the ESM, demonstrating the high PL uniformity of the microporous pixels. In addition, a micro-spectroscopic measurement was conducted to characterize the emission spectrum of each single pixel. The micro-spectroscopy system is illustrated in Fig. S16 in the ESM, and the obtained emission spectra and calculated color coordinates of the pixels are compared in Fig. S17 in the ESM. A high color coordinate stability of the emitting color among pixels is manifested. The enhanced emission intensity and decent homogeneity of the microporous QD pixels illustrate the promising prospect for the industrialization of this approach.

3 Conclusions

In summary, we presented a novel approach for fabricating highly luminescent QD/polymer composites comprising a microporous structure designed for optical scattering and light extraction. This approach combines top–down and bottom–up strategies, by integrating a self-assembly phase separation of the PS and PEG polymer blend with inkjet printing process. Herein, the weight ratio between PS and PEG was selected as the parameter to manipulate the morphology of the microporous network. The resulting microporous structure conferred intensive light scattering property to the QD film, enhancing the light absorption and outcoupling. For the polymer films without QDs, the haze value of the microporous networks ranged from 2.4% to 97.6%. For the QD/polymer composite film, a maximum enhancement of 110% in PL intensity was shown compared to the reference film without the porous structure. By optimizing the ink with the appropriate solvent and polymer concentration, arrays of microporous QD pixel were inkjet printed with adequate uniformity and a regular round shape. The porous QD pixels showed a PL intensity enhancement of 35.3% compared to the sample without micropores. Our approach is versatile and compatible with various QD materials and micro-pattering methods for QD-based display technology. Based on this work, our next step will be dedicated to establishing a full-color display panel with microporous QD pixels.

4 Experimental

Preparation of PS/PEG blend solution: PS polymer (molecular weight: 100,000 Da, Sigma-Aldrich) and PEG polymer (molecular weight: 200 Da, Sigma-Aldrich) polymer were severally solved in chloroform in a concentration of 50 mg/mL, followed by 3 h of magnetic stirring. Then the obtained PS and PEG solutions are mixed according to the desired weight ratio by controlling the volume via pipette. For instance, to prepare 10 mL of PEG-10% solution, 9 mL of PS solution and 1 mL of PEG solution were mixed and followed by 30 min of magnetic stirring.

Preparation of QD/PS/PEG hybrid solution: For drop-casting, PS and PEG were first severally solved in chloroform in a concentration of 100 mg/mL and then mixed with the desired ratio. Subsequently, green emission CdSe/ZnS core–shell QDs powder (Beida Jubang Co., Ltd) was dispersed in chloroform in a concentration of 2 mg/mL and added into the obtained PS/PEG blend solution with a volume ratio of 1:1. Finally, 30 min of magnetic stirring was applied for better homogeneity. For inkjet printing, PS and PEG were solved in 1,2-dichlorobenzene (concentration: 20 mg/mL) and then mixed with QD/1,2-dichlorobenzene dispersion (concentration: 1 mg/mL) with a volume ratio of 1:1.

Drop-casting process: The 16 mm × 16 mm glass substrates (soda lime glass) were cleaned in an ultrasonic bath in acetone and isopropanol for 10 min each, followed by oxygen plasma treatment in a plasma chamber (PlasmaFlecto 30, Plasma technology) with a power of 100 W for 10 min. The solutions were drop-cast on the glass substrates by pipette with a volume of 180 μL. Subsequently, the drop-cast solutions were covered by glass culture dishes with a diameter of 35 mm to prevent gas flow. The temperature of the ambient environment was 22 °C. Consequently, the solidified microporous films were left on the glass substrates after 2 h of solvent volatilization and could be peeled off directly.

Inkjet printing process: Before inkjet printing, glass substrates (20 mm × 20 mm) were cleaned in an ultrasonic bath in acetone and isopropanol for 10 min each. Then polydimethylsiloxane (SYLGARD 184, Sigma-Aldrich) thin film was spin-coated on the glass substrates with a spinning speed of 2000 rpm. During printing, the inkjet printer (PixDro LP50) was equipped with a 10 pl cartridge (Fujifilm Dimatix). Only one nozzle was used for jetting. The substrate temperature was set at 25 °C and the nozzle temperature was 27 °C. The waveforms were single-peak waveforms with a maximum voltage of 20 V and the jetting frequency was 1 kHz. The printing resolution was 200 dots per inch. After the printing, the samples were left in an ambient environment (22 °C) for 10min of natural drying.

Characterizations: The cross-sectional SEM images and the tilted SEM images of the microporous films were observed by JCM-5700 (JEOL) at 10 kV. Before SEM observation, the film samples were immersed in liquid nitrogen for 5 min and

subsequently broken to expose the neat cross-sections. The AFM images of the printed QD pixel were scanned by JPK nanoWizard II atomic force microscope in intermittent contact mode under ambient conditions and analysed with Gwyddion. The overall transmittance and diffuse transmittance spectrum of the films were obtained by PerkinElmer Lambda 1050 UV–VIS–NIR spectrometer with an attached integrating sphere. The diffuse transmittance and haze spectra were measured with the back lid of the integrating sphere opened. The diameter of the integrating sphere of the UV–VIS–NIR spectrometer is 150 mm and the diameter of the back lid is 25 mm. The measurements of PL intensity, PLQY, and absorption of QD films followed the 3M measuring procedure [36, 37] and the illustration of the measuring system is shown in Fig. S6 in the ESM. All the measurements included three samples for each parameter and these results were averaged. The measurements were conducted on a homebuilt optical system. This optical system consists of a laser diode (DL-7146-101S, Roithner Lasertechnik GmbH) with a peak wavelength of 405 nm as an excitation, an integrating sphere with a diameter of 150 mm (Labsphere), and a charge-coupled device spectrometer (AvaSpec-ULS2048x64-TEC, Avantes BV). During the measurements, samples were placed in the middle of the integrating sphere. The laser diode was driven by a laser diode controller (ITC4001, Thorlabs GmbH) and the laser power was 2.5 mW. To measure the angular intensity distribution of the transmitted light through the films, an optical system consisting of a UV–VIS–NIR spectrometer (HR2000CG-UV-NIR, Ocean Optics), a red laser diode (640 nm), and a rotary stage driven by a motion controller (SMC 100PP, Newport) was built as illustrated in Fig. S3 in the ESM. The samples and laser were fixed on the rotation platform and rotated with a step of 2.5° during the measurement. The spectrometer stood still behind the samples for collecting the transmitted light at each rotation step. The microscopic images were obtained by an imaging fluorescence microscope (Zeiss Axioplan).

Acknowledgements

The authors gratefully acknowledge support from the Karlsruhe School of Optics & Photonics and the China Scholarship Council. This research has also been funded by the Deutsche Forschungsgemeinschaft (DFG, German Research Foundation) under Germany's Excellence Strategy via the Excellence Cluster 3D Matter Made to Order (EXC-2082/1-390761711) and through the DFG priority program SPP 1839 "Tailored disorder".

Funding note: Open Access funding enabled and organized by Projekt DEAL

Electronic Supplementary Material: Supplementary material (microscopic images of two-dimensional QD/PS/PEG composite film, cross-sectional SEM images of microporous film cured at different temperature, schematic of the angular distribution measurement and normalized angular distribution of the microporous film, optical properties of QD dispersions, schematic of the PLQY measurement, transmittance and haze spectra of PEG film, characterizations of TiO_2-embedded films, EL spectra of the WLEDs, contact angle measurement of the polydimethylsiloxane interlayer, characterizations of the morphology and luminescence uniformity of QD pixels, and micro-spectroscopy measurement of QD pixels) is available in the online version of this article at https://doi.org/10.1007/s12274-024-6671-9.

References

[1] Smith, M. J.; Lin, C. H.; Yu, S. T.; Tsukruk, V. V. Composite structures with emissive quantum dots for light enhancement. *Adv. Opt. Mater.* **2019**, *7*, 1801072.

[2] García de Arquer, F. P.; Talapin, D. V.; Klimov, V. I.; Arakawa, Y.; Bayer, M.; Sargent, E. H. Semiconductor quantum dots: Technological progress and future challenges. *Science* **2021**, *373*, eaaz8541.

[3] Shu, Y. F.; Lin, X.; Qin, H. Y.; Hu, Z.; Jin, Y. Z.; Peng, X. G. Quantum dots for display applications. *Angew. Chem., Int. Ed.* **2020**, *59*, 22312–22323.

[4] Yang, J.; Choi, M. K.; Yang, U. J.; Kim, S. Y.; Kim, Y. S.; Kim, J. H.; Kim, D. H.; Hyeon, T. Toward full-color electroluminescent quantum dot displays. *Nano Lett.* **2021**, *21*, 26–33.

[5] Wu, X. G.; Ji, H. L.; Yan, X. L.; Zhong, H. Z. Industry outlook of perovskite quantum dots for display applications. *Nat. Nanotechnol.* **2022**, *17*, 813–816.

[6] Anwar, A. R.; Sajjad, M. T.; Johar, M. A.; Hernández-Gutiérrez, C. A.; Usman, M.; Łepkowski, S. P. Recent progress in micro-LED-based display technologies. *Laser Photonics Rev.* **2022**, *16*, 2100427.

[7] Liu, Z. J.; Lin, C. H.; Hyun, B. R.; Sher, C. W.; Lv, Z. J.; Luo, B. Q.; Jiang, F. L.; Wu, T.; Ho, C. H.; Kuo, H. C. et al. Micro-light-emitting diodes with quantum dots in display technology. *Light: Sci. Appl.* **2020**, *9*, 83.

[8] Wei, C. T.; Su, W. M.; Li, J. T.; Xu, B.; Shan, Q. S.; Wu, Y.; Zhang, F. J.; Luo, M. M.; Xiang, H. Y.; Cui, Z. et al. A universal ternary-solvent-ink strategy toward efficient inkjet-printed perovskite quantum dot light-emitting diodes. *Adv. Mater.* **2022**, *34*, 2107798.

[9] Roh, H.; Ko, D.; Shin, D. Y.; Chang, J. H.; Hahm, D.; Bae, W. K.; Lee, C.; Kim, J. Y.; Kwak, J. Enhanced performance of pixelated quantum dot light-emitting diodes by inkjet printing of quantum dot-polymer composites. *Adv. Opt. Mater.* **2021**, *9*, 2002129.

[10] Fan, J. P.; Qian, L. Quantum dot patterning by direct photolithography. *Nat. Nanotechnol.* **2022**, *17*, 906–907.

[11] Myeong, S.; Chon, B.; Kumar, S.; Son, H. J.; Kang, S. O.; Seo, S. Quantum dot photolithography using a quantum dot photoresist composed of an organic–inorganic hybrid coating layer. *Nanoscale Adv.* **2022**, *4*, 1080–1087.

[12] Li, J. S.; Tang, Y.; Li, Z. T.; Li, J. X.; Ding, X. R.; Yu, B. H.; Yu, S. D.; Ou, J. Z.; Kuo, H. C. Toward 200 lumens per watt of quantum-dot white-light-emitting diodes by reducing reabsorption loss. *ACS Nano* **2021**, *15*, 550–562.

[13] Li, X.; Liu, J. L.; Jiang, G. C.; Lin, X. Y.; Wang, J.; Li, Z. Q. Self-supported $CsPbBr_3/Ti_3C_2T_x$ MXene aerogels towards efficient photocatalytic CO_2 reduction. *J. Colloid Interface Sci.* **2023**, *643*, 174–182.

[14] Yang, H. C.; Zhou, M.; Tang, H. D.; Sun, M. Y.; Liu, P.; Liu, Y. Z.; Chen, L. X.; Li, D. Z.; Wu, D.; Hao, J. J. et al. Enhanced light emission of quantum dot films by scattering of poly(zinc methacrylate) coating CdZnSeS/ZnS quantum dots and high refractive index $BaTiO_3$ nanoparticles. *RSC Adv.* **2020**, *10*, 31705–31710.

[15] Meinardi, F.; Colombo, A.; Velizhanin, K. A.; Simonutti, R.; Lorenzon, M.; Beverina, L.; Viswanatha, R.; Klimov, V. I.; Brovelli, S. Large-area luminescent solar concentrators based on "Stokes-shift-engineered" nanocrystals in a mass-polymerized PMMA matrix. *Nat. Photonics* **2014**, *8*, 392–399.

[16] Li, J. S.; Tang, Y.; Li, Z. T.; Ding, X. R.; Yu, B. H.; Lin, L. W. Largely enhancing luminous efficacy, color-conversion efficiency, and stability for quantum-dot white LEDs using the two-dimensional hexagonal pore structure of sba-15 mesoporous particles. *ACS Appl. Mater. Interfaces* **2019**, *11*, 18808–18816.

[17] Hyun, B. R.; Sher, C. W.; Chang, Y. W.; Lin, Y. H.; Liu, Z. J.; Kuo, H. C. Dual role of quantum dots as color conversion layer and suppression of input light for full-color micro-LED displays. *J. Phys. Chem. Lett.* **2021**, *12*, 6946–6954.

[18] Liang, G. W.; Tang, Y.; Chen, P. S.; Li, J. S.; Yuan, Y. K.; Yu, S. D.; Xu, L.; Li, Z. T. Polystyrene-fiber-rod hybrid composite structure for optical enhancement in quantum-dot-converted light-emitting diodes. *ACS Appl. Polym. Mater.* **2022**, *4*, 91–99.

[19] Yu, S. D.; Zhuang, B. S.; Chen, J. C.; Li, Z. T.; Rao, L. S.; Yu, B. H.; Tang, Y. Butterfly-inspired micro-concavity array film for color conversion efficiency improvement of quantum-dot-based light-emitting diodes. *Opt. Lett.* **2017**, *42*, 4962–4965.

[20] Yin, M. J.; Pan, T.; Yu, Z. W.; Peng, X. M.; Zhang, X.; Xie, W. F.; Liu, S. H.; Zhang, L. T. Color-stable WRGB emission from blue OLEDs with quantum dots-based patterned down-conversion layer. *Org. Electron.* **2018**, *62*, 407–411.

[21] Li, Y. Y.; Yu, S.; Veinot, J. G. C.; Linnros, J.; Berglund, L.; Sychugov, I. Luminescent transparent wood. *Adv. Opt. Mater.* **2017**, *5*, 1600834.

[22] Kumar, P.; Ganesh, N.; Narayan, K. S. Electrospun fibers containing emissive hybrid perovskite quantum dots. *ACS Appl. Mater. Interfaces* **2019**, *11*, 24468–24477.

[23] Theobald, D.; Yu, S. D.; Gomard, G.; Lemmer, U. Design of selective reflectors utilizing multiple scattering by core–shell nanoparticles for color conversion films. *ACS Photonics* **2020**, *7*, 1452–1460.

[24] Yu, B. H.; Lu, Z.; Liang, G. W.; Yuan, Y. K.; Wang, H.; He, J. Q.; Yang, S. Luminous efficacy enhancement for LED lamps using highly reflective quantum dot-based photoluminescent films. *Opt. Express* **2021**, *29*, 29007–29020.

[25] Yu, S. D.; Fritz, B.; Johnsen, S.; Busko, D.; Richards, B. S.; Hippler, M.; Wiegand, G.; Tang, Y.; Li, Z. T.; Lemmer, U. et al. Enhanced photoluminescence in quantum dots-porous polymer hybrid films fabricated by microcellular foaming. *Adv. Opt. Mater.* **2019**, *7*, 1900223.

[26] Kim, G. Y.; Kim, S.; Choi, J.; Kim, M.; Lim, H.; Nam, T. W.; Choi, W.; Cho, E. N.; Han, H. J.; Lee, C. et al. Order-of-magnitude, broadband-enhanced light emission from quantum dots assembled in multiscale phase-separated block copolymers. *Nano Lett.* **2019**, *19*, 6827–6838.

[27] Wang, S. Z.; Yousefi Amin, A. A.; Wu, L. Z.; Cao, M. H.; Zhang, Q.; Ameri, T. Perovskite nanocrystals: Synthesis, stability, and optoelectronic applications. *Small Struct.* **2021**, *2*, 2000124.

[28] Li, J. X.; Li, Z. T.; Qiu, J. Y.; Li, J. S. Photothermal optimization of quantum dot converters for high-power solid-state light sources. *Adv. Opt. Mater.* **2022**, *10*, 2102201.

[29] Hu, Z. P.; Yin, Y. M.; Ali, M. U.; Peng, W. X.; Zhang, S. J.; Li, D. Z.; Zou, T. Y.; Li, Y. Y.; Jiao, S. B.; Chen, S. J. et al. Inkjet printed uniform quantum dots as color conversion layers for full-color OLED displays. *Nanoscale* **2020**, *12*, 2103–2110.

[30] Yang, P. H.; Zhang, L.; Kang, D. J.; Strahl, R.; Kraus, T. High-resolution inkjet printing of quantum dot light-emitting microdiode arrays. *Adv. Opt. Mater.* **2020**, *8*, 1901429.

[31] Zhang, Q. S.; Jin, Q. H.; Mertens, A.; Rainer, C.; Huber, R.; Fessler, J.; Hernandez-Sosa, G.; Lemmer, U. Fabrication of Bragg mirrors by multilayer inkjet printing. *Adv. Mater.* **2022**, *34*, 2201348.

[32] Zhang, Q. S.; Schambach, M.; Schlisske, S.; Jin, Q. H.; Mertens, A.; Rainer, C.; Hernandez-Sosa, G.; Heizmann, M.; Lemmer, U. Fabrication of microlens arrays with high quality and high fill factor by inkjet printing. *Adv. Opt. Mater.* **2022**, *10*, 2200677.

[33] Donie, Y. J.; Schlisske, S.; Siddique, R. H.; Mertens, A.; Narasimhan, V.; Schackmar, F.; Pietsch, M.; Hossain, I. M.; Hernandez-Sosa, G.; Lemmer, U. et al. Phase-separated nanophotonic structures by inkjet printing. *ACS Nano* **2021**, *15*, 7305–7317.

[34] Kim, J. K.; Taki, K.; Ohshima, M. Preparation of a unique microporous structure via two step phase separation in the course of drying a ternary polymer solution. *Langmuir* **2007**, *23*, 12397–12405.

[35] Kim, J. K.; Taki, K.; Nagamine, S.; Ohshima, M. Preparation of a polymeric membrane with a fine porous structure by dry casting. *J. Appl. Polym. Sci.* **2009**, *111*, 2518–2526.

[36] de Mello, J. C.; Wittmann, H. F.; Friend, R. H. An improved experimental determination of external photoluminescence quantum efficiency. *Adv. Mater.* **1997**, *9*, 230–232.

[37] Faulkner, D. O.; McDowell, J. J.; Price, A. J.; Perovic, D. D.; Kherani, N. P.; Ozin, G. A. Measurement of absolute photoluminescence quantum yields using integrating spheres—Which way to go? *Laser Photonics Rev.* **2012**, *6*, 802–806.

[38] Li, J. S.; Tang, Y.; Li, Z. T.; Cao, K.; Yan, C. M.; Ding, X. R. Full spectral optical modeling of quantum-dot-converted elements for light-emitting diodes considering reabsorption and reemission effect. *Nanotechnology* **2018**, *29*, 295707.

[39] Mohan, R.; Drbohlavova, J.; Hubalek, J. Water-dispersible TiO_2 nanoparticles via a biphasic solvothermal reaction method. *Nanoscale Res. Lett.* **2013**, *8*, 503.

[40] Singh, S. P.; Sharma, S. K.; Kim, D. Y. Carrier mechanism of ZnO nanoparticles-embedded PMMA nanocomposite organic bistable memory device. *Solid State Sci.* **2020**, *99*, 106046.

[41] Auger, J. C.; McLoughlin, D. Theoretical analysis of light scattering properties of encapsulated rutile titanium dioxide pigments in dependent light scattering regime. *Prog. Org. Coat.* **2014**, *77*, 1619–1628.

[42] Jin, Q. H.; Zhang, Q. S.; Chen, J. C.; Gehring, T.; Eizaguirre, S.; Huber, R.; Gomard, G.; Lemmer, U.; Kling, R. High dynamic range smart window display by surface hydrophilization and inkjet printing. *Adv. Mater. Technol.* **2022**, *7*, 2101026.